batteries

MDPI

Article

Propane Ignition Characteristics in a Pt-Catalyzed Microreactor for SOFC Preheating: A Numerical Study of Catalyst Activity Effects

Zhulong Wang [1], Zhen Wang [1], Zhifang Miao [2], Lili Ma [1], Weiqiang Xu [1], Zunmin Li [1,*], Zhiyuan Yang [3] and Guohe Jiang [3]

[1] Ocean College, Binzhou Polytechnic, Binzhou 256603, China
[2] College of Chemical Engineering and Energy, Binzhou Polytechnic, Binzhou 256603, China
[3] Merchant Marine College, Shanghai Maritime University, Shanghai 201306, China
* Correspondence: lizunmin1@bzpt.edu.cn

Abstract

Leveraging catalytic microreactors as compact yet powerful thermal sources represents a promising approach to enable rapid and reliable startup of small-scale solid oxide fuel cell (SOFC) systems. In the present study, the homogeneous–heterogeneous (HH) combustion behavior of a propane/air mixture in a Pt-catalyzed microreactor is investigated using two-dimensional computational fluid dynamic (CFD) simulations. The catalytic reaction kinetics model is integrated into the general module of ANSYSY Fluent via a user-defined function (UDF) interface. By varying the surface area factor, the ignition characteristics of the propane/air mixture under different catalyst activities are systematically explored. Numerical results reveal that the relative catalyst activity range of 0–2 represents a sensitive region for propane/air ignition characteristics, characterized by a 541 K decrease in ignition temperature and a 50% reduction in ignition delay time. Nevertheless, further increases in relative catalyst activity from 2 to 10, yield a much smaller reduction—64 K in ignition temperature and 6.7 s in ignition delay time—indicating a weakly responsive regime. The relative contribution of the heterogeneous reaction (HTR) to the total heat release decreases with higher feed temperatures but increases with enhanced catalyst activity. Regarding the temporal evolution of HTR contribution, the initiation of homogeneous ignition undermines the dominance of HTR contribution. Irrespective of catalytic activity levels, the relative contributions of the two reaction pathways subsequently undergo dynamic redistribution and ultimately stabilize, reaching an equilibrium state within approximately 10 s. These findings provide critical insights into the role of catalyst activity in propane/air mixture ignition and the interplay between homogeneous and heterogeneous reactions in microscale combustion systems.

Keywords: catalytic microreactors; ignition temperature; ignition delay time; catalytic activity; homogeneous–heterogeneous combustion

Academic Editor: Piercarlo Mustarelli

Received: 26 August 2025
Revised: 4 October 2025
Accepted: 14 October 2025
Published: 23 October 2025

Citation: Wang, Z.; Wang, Z.; Miao, Z.; Ma, L.; Xu, W.; Li, Z.; Yang, Z.; Jiang, G. Propane Ignition Characteristics in a Pt-Catalyzed Microreactor for SOFC Preheating: A Numerical Study of Catalyst Activity Effects. *Batteries* **2025**, *11*, 390. https://doi.org/10.3390/batteries11110390

1. Introduction

Solid oxide fuel cells (SOFCs) have gained remarkable attention as a next-generation power generation technology due to their high electrical efficiency (the net electrical efficiency can reach 60% and the combined thermal and electrical efficiency can reach about 90%), fuel flexibility (can directly use various fuels such as hydrogen, natural gas, ammonia gas, and biomass gas for power generation), and low emissions [1–5]. However, the

industrial scale-up of this system is hindered by a critical challenge: the high operating temperature (generally between 500 and 1000 °C) requires a prolonged startup time and significant energy input for preheating [3,4,6]. The conventional preheating strategy employs electric heaters, which creates a fundamental dependency on an external electrical source, either from the grid or an auxiliary battery. This reliance severely compromises the independent capability and energy efficiency of the SOFC system.

A standalone catalytic microreactor offers a promising solution to the startup of small-scale SOFCs. This dedicated heating unit enables rapid, localized, and on-demand thermal management, significantly reducing startup time and energy overhead while improving system reliability and flexibility [7,8]. The unique micro-scale structure of catalytic microreactors enables efficient heat and mass transfer, significantly enhancing combustion efficiency while minimizing pollutant emissions [9–13]. Compared with traditional combustion modes, it achieves more complete fuel oxidation at lower temperatures, effectively suppressing the formation of nitrogen oxides and unburned hydrocarbons [14]. Moreover, the compact design of microreactors allows for a smaller reactor volume, facilitating system miniaturization and integration, which is particularly crucial for applications in portable power generation and distributed energy systems [15–19].

In catalytic microreactors, there exist homogeneous gas-phase reactions and heterogeneous surface reactions [17,20]. Homogeneous gas-phase reactions occur within the bulk gas phase, driven by thermodynamics and kinetics, where reactant molecules react freely in the gas environment. Meanwhile, heterogeneous surface reactions take place on the surface of the catalyst. The catalyst provides active sites, lowering the activation energy of the reaction. Reactants are adsorbed onto these active sites, undergo chemical transformations, and then desorb as products. The relationship between these two reaction types in a micro-catalytic reactor is complex, as they are interconnected and can either enhance each other's performance synergistically or negatively impact one another through competition [20–22]. The synergy between gas-phase and surface reactions manifests as the heat released by one promoting the other. The competition arises from the race for a limited supply of reactants. This interplay of synergistic thermal effects and competitive reactant acquisition determines the overall reaction efficiency and product distribution. Undoubtedly, advancing the understanding of the underlying mechanisms is crucial for the design and optimization of catalytic microreactor systems across various chemical and energy-related applications.

A practically significant aspect of catalytic microreactor research involves the optimization of structural design. The overall geometry, including the aspect ratio of the combustion chamber, the specific configuration (e.g., straight channels, Swiss-roll, serpentine paths, annular designs), and the presence of internal features like fins or porous media, profoundly influences flow dynamics, heat transfer, and residence time [19,20,23–25]. Specific parameters such as gap size (the distance between opposing walls or catalyst layers) and wall thickness are particularly important. At a constant inlet velocity, an increase in the gap size induces a reduction in the ignition temperature and an elevation in the maximum temperature [24]. Under conditions of constant intake mass flow, variations in gap size are found to have negligible effects on the ignition temperature and the ignition delay [17]. Nevertheless, increasing the gap size would occupy more space, thereby affecting the overall geometric configuration of microburners. The wall thickness impacts the thermal resistance of the reactor walls and heat absorption during the system's heating process. The ignition time and the time for the system to reach a stable state increase with an increase in wall thickness. Furthermore, wall thickness can affect the wall temperature distribution. A thicker wall usually leads to a more uniform wall temperature distribution. Research often explores trade-offs between these parameters to achieve optimal performance, such as

maximizing thermal efficiency or minimizing pollutant formation. The studies on narrow slit-type microreactors highlight the sensitivity of combustion characteristics to geometric details, emphasizing the need for precise control over dimensions to ensure stable and efficient operation.

The washcoat effect has also been shown to be a crucial aspect in determining the performance of catalytic microreactors. Herdem et al. developed a detailed model of a methane steam reformer incorporating transport phenomena within the washcoat layer, and proposed a segmented catalyst structure to enhance reactor performance [26,27]. Cao et al. numerically investigated the effects of washcoat properties on a plate microchannel reactor for steam methane reforming [28]. Using a detailed computational model, the study found that pore size was a key factor in managing heat transfer and temperature distribution, while porosity played a minor role. Similarly, Liu et al. developed a washcoat-resolved model of a catalytic micro-combustor for methane–air combustion [29]. The findings determined that washcoat thickness required a balance: an overly thin layer weakened catalytic reactions, whereas an overly thick one caused severe diffusion limitations and low catalyst utilization. The study further concluded that porosity, pore size, and tortuosity collectively influenced combustion by modifying mass transport.

Beyond the physical design, the performance of catalytic microreactors is highly sensitive to operational control conditions. Key parameters include feed temperature, equivalence ratio, and mass flow rate [18,30–32]. The feed temperature is crucial for overcoming the ignition barrier and maintaining the catalyst above its light-off temperature. Preheating the reactants, often above the auto-ignition temperature of the fuel by 100–150 °C, is a common practice to ensure rapid and complete ignition. Operating the catalyst at its optimal temperature range maximizes conversion efficiency while avoiding deactivation at excessively high temperatures. The equivalence ratio of the incoming stream directly influences combustion efficiency and emission levels. Operating at stoichiometric or slightly fuel-rich conditions generally promotes complete combustion [32]. Fuel-lean conditions may lead to ignition difficulties, while fuel-rich conditions tend to produce soot or unburned hydrocarbons. Additionally, well-controlled operating parameters are needed to avoid conditions that can result in catalyst poisoning or deactivation. The mass flow rate affects residence time and convective heat transfer [33]. Higher flow rates can cause flame blow-off due to shortened residence time, while lower flow rates may lead to local quenching and combustion instability. In practical applications, precise control over these parameters is essential for stable operation, efficient energy conversion, and low emissions, often achieved through automated systems that monitor and adjust conditions in real-time.

Selecting structural materials and catalyst for microreactors is another critical research area, as these materials influence performance through their physical and chemical properties. The wall thermal conductivity is a key factor in heat management [18,34,35]. Materials with high thermal conductivity (e.g., certain metals) can facilitate efficient heat recirculation from the reaction zone to the inlet, helping to sustain combustion and reduce ignition energy requirements. However, excessive conductivity can also lead to rapid heat loss to the environment. Structural materials with low thermal conductivity (e.g., ceramics or insulating layers) may retain heat within the reactor, potentially leading to localized hot spots. The material's thermal stability at high temperatures is also vital to prevent degradation or structural failure. The properties of the catalyst material—specifically surface area, pore structure, and active metal composition—are critical, as they govern catalytic activity, selectivity, and poisoning resistance [9,36,37]. Extensive studies have been conducted on various catalyst compositions and support structures [38,39]. Notable examples include monolithic catalysts incorporating precious metals such as platinum (Pt), palladium (Pd), and rhodium (Rh), as well as base metal oxides supported on high-surface-area materials

like porous alumina, silicon carbide ceramics, and metallic foams [40,41]. These supports provide not only mechanical stability but also a large surface area for catalyst dispersion, crucial for maximizing catalytic activity. Research has demonstrated the effectiveness of these catalysts in promoting the combustion of hydrocarbon fuels, including methane (CH_4), hydrogen (H_2), and propane (C_3H_8), by significantly lowering ignition temperatures and ensuring stable reaction pathways [42,43]. The performance of these catalysts is typically evaluated based on activity, operational temperature range, and reaction stability.

In summary, while previous studies have extensively investigated the ignition performance in microreactors in terms of structural designs, operating conditions, physical property parameters, and novel catalyst development, the impact of catalyst activity—a lumped parameter that accounts for tangible properties such as loading, dispersion, and specific surface area of the support—warrants further systematic investigation. The presented paper fits in this framework to gain insight into the role of catalytic activity in ignition and combustion characteristics of a propane/air mixture within microreactors. The organization of this paper is as follows. Section 2 presents the microreactor geometry, operating conditions, and specifics of the CFD simulations. Section 3 presents the simulation results and discussion regarding the impact of catalyst activity on propane's ignition and combustion characteristics. Lastly, Section 4 provides a summary of the present study's conclusions.

2. Mathematical Model

2.1. Model Description

This study utilizes a straight-through, single-channel microreactor measuring 20 mm in length, 0.5 mm in channel width, and 0.05 mm in wall thickness. The inner wall surface of the reactor is uncoated with active catalyst for the initial 1 mm, while the remaining 19 mm is coated with active catalyst. Due to the symmetry between the two plates, only half of the reactor is extracted for simulation. Figure 1 shows the two-dimensional computational domain of the microreactor.

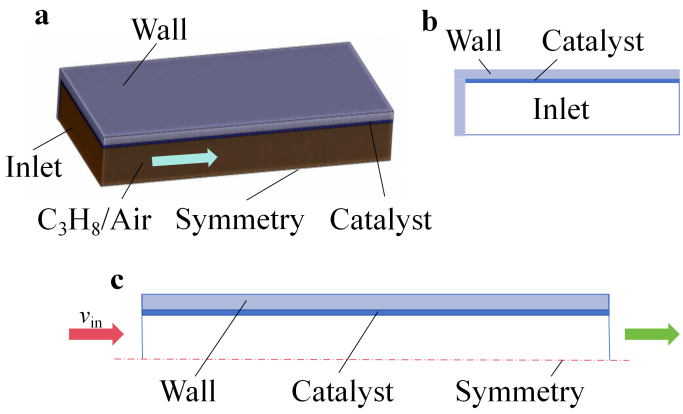

Figure 1. Scheme of the rectangular microreactor (**a**), cross section (**b**), and longitudinal section (**c**) of the computational domain.

The mathematical model is derived based on the following assumptions:

(1) The flow in the microchannel is assumed to be laminar;
(2) The gas mixture is treated as an ideal gas;
(3) Radiation effects from the gas phase are neglected;
(4) Heat losses from the walls are described using Newton's law of cooling, with the influence of surface radiation incorporated into an effective heat transfer coefficient.

The governing equations in the numerical computation are described below.

Continuity equation:

$$\frac{\partial \rho_g}{\partial t} + \nabla \cdot (\rho_g V) = 0 \tag{1}$$

where ρ_g is the gas mixture density, and V represents the velocity vector.

Momentum balance:

$$\frac{\partial (\rho_g V)}{\partial t} + \nabla \cdot (\rho_g V V) = -\nabla P + \nabla \cdot \mu \left[\left(\nabla V + (\nabla V)^T - \frac{2}{3} (\nabla \cdot V) I \right) \right] \tag{2}$$

where P stands for the pressure, and μ denotes the dynamic viscosity.

Gas phase energy balance:

$$\frac{\partial (\rho_g h_g)}{\partial t} + \nabla \cdot (\rho_g h_g V) = \nabla \cdot \left(\lambda_g \nabla T - \sum_i^{n_{gpc}} h_i J_i \right) + \sum_i^{n_{gpc}} h_i R_i^{gas} \tag{3}$$

where h_g is the gas enthalpy, and λ_g stands for the gas thermal conductivity, and n_{gpc} represents the number of gas phase components, and J_i indicates the diffusion flux of the i-th component, and R_i denotes the generation rate of the i-th component.

Solid energy balance:

$$\frac{\partial (\rho_s h_s)}{\partial t} = \nabla \cdot (\lambda_s \nabla T) \tag{4}$$

where ρ_s is the density of the solid wall, and h_s indicates the solid enthalpy, and λ_s stands for the solid thermal conductivity.

Species balance equation:

$$\frac{\partial (\rho_g Y_i)}{\partial t} + \nabla \cdot (\rho_g Y_i V + J_i) = R_i^{gas} \tag{5}$$

where Y_i is the mass fraction of the i-th component.

The global reaction equation for propane oxidation is as follows:

$$C_3H_8 + 5O_2 \rightarrow 3CO_2 + 4H_2O \tag{6}$$

The homogeneous reaction kinetics of propane are modeled using the one-step global mechanism developed by Westbrook and Dryer [44].

$$r_{homo} = 4.836 \times 10^9 e^{\left(-\frac{1.256 \times 10^8}{RT}\right)} c_{C_3H_8}^{0.1} c_{O_2}^{1.65} \tag{7}$$

where c represents the molar concentration with a unit of $kmol/m^3$, and r_{homo} denotes the homogeneous reaction rate with a unit of $kmol/(m^3 \cdot s)$.

The heterogeneous reaction kinetics of propane follow a single-step reduced-order mechanism developed by Deshmukh and Vlachos [45], which is in good agreement with the full model, as well as with experimental data (both catalyst ignition and autothermal fixed-bed data).

$$r_{hete} = \frac{\eta k_{C_3H_8}^{ads} X_{C_3H_8}}{\left(1 + \sqrt{\frac{k_{O_2}^{ads} X_{O_2}}{k_{O_2}^{des}}}\right)^2} \tag{8}$$

where η is the surface area factor, and X stands for the mole fraction, and k^{ads} represents the adsorption rate constants, and k^{des} indicates the desorption rate constants. k^{ads} and k^{des} are computed by the following expressions.

$$k_i^{\mathrm{ads}} = \frac{s_i P_{\mathrm{tot}} \mathrm{e}^{-E_{\mathrm{a},i}^{\mathrm{ads}}/RT}}{\Gamma\sqrt{2\pi M_i RT}} \left(\frac{T}{T_{\mathrm{ref}}}\right)^{\beta_i^{\mathrm{ads}}} \tag{9}$$

$$k_i^{\mathrm{des}} = A_i \mathrm{e}^{-E_{\mathrm{a},i}^{\mathrm{des}}/RT} \left(\frac{T}{T_{\mathrm{ref}}}\right)^{\beta_i^{\mathrm{des}}} \tag{10}$$

where s, R, P_{tot}, Γ, M, T_{ref}, β, E_{a}, and A represent the sticking coefficient, the ideal gas constant, the total pressure, the active site density of the catalyst, the molecular weight, the reference temperature, the temperature exponent, the activation energy, and the pre-exponential factor, respectively.

The kinetic parameters in Equations (8)–(10) are adopted from Ref. [45]. The sticking coefficient (s), temperature exponent (β), and activation energy (E_{a}) for propane adsorption are 0.06 s^{-1}, 0.154, and 4 kcal/mol, respectively. For oxygen adsorption, the corresponding values are 0.0542 s^{-1}, 0.766, and 0 kcal/mol. For the oxygen desorption process, the pre-exponential factor (A) and temperature exponent are 8.41×10^{12} s^{-1} and -0.796, respectively, while the activation energy is given by Equation (11). In addition, a surface area factor of 1.7 and an active site density of 2.9×10^{-9} mol/cm^2 are used.

$$E_{\mathrm{O_2}}^{\mathrm{des}} = 0.126T_{\mathrm{r}}^4 - 1.849T_{\mathrm{r}}^3 + 9.142T_{\mathrm{r}}^2 - 13.253T_{\mathrm{r}} + 23.903 \tag{11}$$

Here, $T_{\mathrm{r}} = T/T_{\mathrm{ref}}$ denotes the temperature ratio.

2.2. Meshing, Boundary Conditions, Physical Properties, and Solution Strategy

The computational domain is discretized into 200,000 quadrilateral grid cells, using a distribution of 2001 nodes in the axial direction and 101 nodes in the radial direction. The grid spacing is designed to ensure adequate solving precision for both the gas flow and the solid region, with progressive refinement from an initial coarse mesh of 50,000 cells. Mesh independence is verified when further increases in node density yields negligible changes in ignition characteristics (e.g., ignition temperature and ignition delay time).

Dirichlet boundary conditions are implemented at the reactor entrance. A velocity condition is applied at the inlet boundary with a fixed value of 2 m/s. The feed stream is specified to be a mixture of propane and air with an equivalence ratio of 0.6. A pressure boundary condition is applied at the outlet with a constant value of 1 atm (101.325 kPa). No-slip condition is enforced at every fluid–solid interface. A convective heat transfer boundary condition is applied to the outer wall, featuring a heat transfer coefficient of 20 $\mathrm{W}/(\mathrm{m}^2 \cdot \mathrm{K})$ and a free steam temperature of 300 K. The heat dissipation from the microreactor's exterior wall occurs in accordance with Newton's law of cooling.

The density variation is calculated via the ideal gas law. The thermal conductivity and viscosity of the mixture are computed using the mass-weighted mixing law. The mass diffusivity is determined through kinetic theory. The transport properties of individual species are derived from kinetic theory. The specific heat of each species is computed based on a piecewise polynomial relation. For the solid, the specific heat and thermal conductivity are taken as constant, with values of 503 $\mathrm{J}/(\mathrm{kg}\cdot\mathrm{K})$ and 20 $\mathrm{W}/(\mathrm{m}\cdot\mathrm{K})$, respectively. In order to modulate the catalyst activity, the surface area factor η is designated as a control variable. We scale η to obtain η', and define the scaling factor, i.e., the ratio of η' to the baseline value of η, as the relative catalytic activity γ_{cat}. The present study employs a series of scaling factors ranging from 0.1 to 10 to examine the effect of the catalyst activity on the ignition characteristics of the propane/air mixture. A value of γ_{cat} = 0.1 represents a

catalyst with low loading, poor dispersion (low active site density), or a sintered surface (reduced effective surface area). A value of γ_{cat} = 10 represents an ideal, highly active state with high dispersion, optimal loading, and a large effective surface area. Thus, the range of 0.1 to 10 spans from a severely degraded catalyst to an optimally active one, covering realistic variations in these physical properties.

The ANSYS Fluent package [46] serves as the numerical solver for the computational fluid dynamics (CFD) simulations in this study. The subroutine for the kinetic rate model of heterogeneous reaction is incorporated through the user-defined function (UDF) interface. The second-order upwind scheme is adopted to discretize the convection terms in the governing equations. Algorithm SIMPLE is employed to handle the coupling between pressure and velocity. For the transient simulation, the time step sensitivity analysis confirms that a time step size of 0.01 s ensures time step independence. The convergence is confirmed by examining the residuals, flux balances, and monitors. The criteria for time step advancement requires the residual of the energy conservation equation to be below 10^{-8} and the residuals for other equations to be below 10^{-4}, with the stabilization of temperature and propane mass fraction at the monitoring points.

2.3. Model Validation

To ensure the reliability and accuracy of the mathematical model employed in this study, we perform validation by comparing the results of numerical simulations with experimental data reported in Reference [32]. In the experiment, the authors used a microcombustor with internal dimensions of 20 mm in length, 3 mm in height, and 10 mm in width. The flat panels of the combustor were made of steel with a specific heat capacity of 503 $J/(kg{\cdot}K)$. The inner surfaces of the flat panels were coated with platinum at a surface site density of 2.7063×10^{-9} mol/cm^2. A premixed propane/air mixture was introduced into the combustor through a square-shaped inlet on one side of the channel.

Figure 2 compares the outer-wall temperature distributions of the catalytic combustor obtained from the numerical simulation and experimental measurements at an inlet velocity of 0.3 m/s and an equivalence ratio of 1.0, representing a typical operating condition. As can be observed, the variation trend exhibited by the simulation predictions aligns closely with that of the experimental results. The position where the temperature reaches its maximum value was correctly predicted by the numerical model, in agreement with experimental data. At corresponding positions, the two wall temperature profiles exhibit a maximum deviation of 27 K, with a relative error of 3.1%. The discrepancies between the simulated and experimentally measured results may be attributed to simplifications in the chemical reaction mechanism, i.e., the use of a single-step global reaction model, which tends to overpredict temperature values. Additionally, the neglect of detailed catalyst coating morphology in the model may also contribute to these deviations. Nevertheless, such a small error provides strong evidence that the numerical model, along with the associated chemical mechanisms and physical assumptions, is valid and can be reliably used for further investigations into the performance and characteristics of the catalytic microreactor.

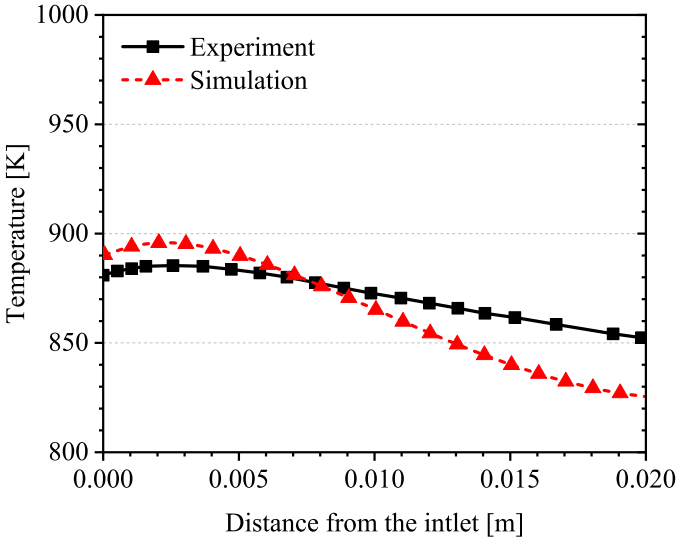

Figure 2. Comparison of the outer wall temperature distribution: numerical simulation vs. experimental measurement.

3. Results and Analysis

As a preliminary step, steady-state calculations are carried out to determine the ignition temperatures for propane/air mixture under various catalyst activities. Subsequently, transient simulations are run with feed temperatures set 10 K above the previously determined ignition temperatures (a slight superheating above the minimum ignition temperature is representative of practical system operation, where a safety margin or a preheating stage would be used to ensure stable ignition). Notably, we perform steady-state simulations to identify the respective ignition temperature at each catalyst activity level, starting from an initial feed temperature of 300 K.

3.1. Determination of Ignition Temperature for Different Catalyst Activities

Figure 3 shows the maximum temperature as a function of feed temperature for relative catalyst activities of 0.5, 1, 2 and 5. For each catalyst activity level, a key observation is the presence of a turning point during the rise in feed temperature, where the maximum temperature experiences a sharp increase. Below this point, the maximum temperatures are approximately equal to the feed temperatures, indicating unignited states. Above this point, the maximum temperatures are substantially higher than the feed temperatures and rise further as the feed temperature is increased. Notably, this turning point defines the ignition temperature, i.e., the minimum feed temperature required for propane/air mixture combustion startup. Another finding from this figure is that, at the same feed temperature (above the ignition temperature), the maximum temperature decreases as the catalyst activity increases. This suggests that higher catalyst activity reduces the combustion temperature inside the microreactor. The underlying cause for this will be elaborated upon later. Additionally, despite a reduced fuel flow rate due to higher feed temperature, the maximum temperature exhibits a consistent rise with increasing feed temperature.

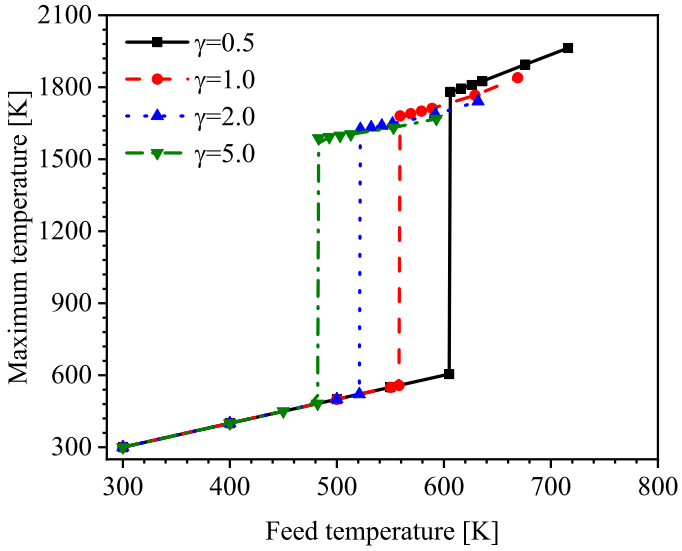

Figure 3. Maximum temperature as a function of feed temperature.

3.2. Effect of Catalyst Activity on the Ignition Temperature and Maximum Temperature

Figure 4 shows ignition temperatures (solid line) and maximum temperatures (dashed line) for the propane/air mixture at various relative catalyst activities.

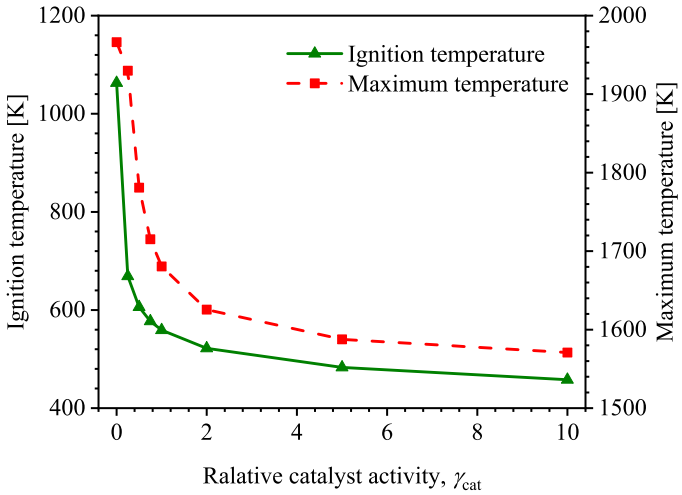

Figure 4. Dependence of ignition temperature on relative catalyst activity.

Evidently, the ignition temperature exhibits a decreasing trend as the relative catalyst activity rises. The boost in catalyst activity resulting from an increase in the surface area factor facilitates heat buildup for ignition. Specifically, when the relative catalyst activity increases from 0 to 1, and then to 10, the ignition temperature decreases from 1063 K to 559 K, and then to 458 K. This clearly demonstrates the strong dependence of ignition temperature on catalyst activity, which identifies catalytic reaction kinetics as the dominant factor governing propane/air mixture ignition behavior. As a result, the catalytic reaction acts as a precursor to propane/air mixture combustion. In addition, the relative catalyst activity range of 0–2 represents a sensitive regime for propane/air mixture ignition behavior, characterized by a sharp 541 K decrease in ignition temperature (from 1063 K to 522 K), while further increasing the activity to 10 yields only an additional 64 K reduction (from 522 K to 458 K), demonstrating diminishing returns at higher activity levels. The underlying mechanism lies in the transition from kinetic control to a diffusion-limited regime, suggesting an optimal operational window at relative catalyst activities below 2.

In addition, the maximum temperature decreases with increasing catalyst activity, mirroring the trend observed for ignition temperature, indicating that higher catalyst activity suppresses the combustion temperature of the propane-air mixture. This result is qualitatively consistent with the findings reported in Reference [17] exploring the role of homogeneous reaction in the ignition characteristics of a propane/air mixture in a Pt-catalyzed microburner, which demonstrated that maximum temperatures are significantly lower in the absence of homogeneous reaction compared to HH combustion conditions. The underlying mechanism stems from heat transfer dynamics and the stark difference in volumetric heat capacities between the gas and solid. The heterogeneous reaction taking place on the solid surface allows the released heat to be efficiently conducted to the adjacent solid wall. For example, as derived from our calculations, a net increase of 49 W is manifested in the area-integrated heat flux across the catalytic gas–solid interface when the relative activity is elevated from 1 to 5. Nevertheless, the volumetric heat capacity of the solid material is three orders of magnitude higher than that of the gas mixture. Thus, the solid phase exhibits a less pronounced temperature rise than the gas phase given equal heat absorption. This directly explains the observed reduction in maximum temperature.

3.3. Effect of Catalyst Activity on the HTR Contribution

Figure 5 shows HTR contributions (defined as the ratio of the fuel consumption rate due to the heterogeneous reaction to the total fuel consumption rate) at various relative catalyst activities. It can be observed that the HTR contribution increases with enhanced catalyst activity. As discussed previously, catalytic reaction kinetics plays a decisive role in the ignition temperature. Increasing catalyst activity lowers the ignition temperature, thereby suppressing the maximum temperature in the microreactor. A decrease in the overall temperature reduces the rates of both homogeneous and heterogeneous reactions. However, as evidenced by the simulation results, the homogeneous reaction shows greater sensitivity to temperature variations. Prior to ignition, the catalytic pathway dominates reactant consumption. Nevertheless, as the catalytic reaction progresses, the heat release from catalytic reaction elevates the temperature to the critical threshold required for homogeneous combustion initiation, after which the two reaction pathways compete. Furthermore, the reaction may transition from kinetic control to diffusion control with increasing catalyst activity due to mass transfer limitations. In this scenario, the rate of reactant diffusion to the catalyst surface becomes the bottleneck, thereby creating space for the homogeneous reaction. As a result, the rise in the HTR contribution tends to slow down with further increases in catalyst activity, as shown in the figure.

Figure 6 examines how catalyst activity and feed temperature influence the HTR contribution in the catalytic microreactor. The figure demonstrates several key trends in the HTR contribution under different conditions. Across all four catalyst activity levels, the HTR contribution consistently decreases with increasing feed temperature. This thermal dependence arises because the homogeneous reaction exhibits greater temperature sensitivity compared to the heterogeneous counterpart, resulting in an increased contribution of homogeneous reaction pathway at elevated temperatures. Given an identical feed temperature, higher catalyst activity results in greater HTR contribution. This positive correlation stems from the kinetic enhancement of heterogeneous reaction when catalyst activity improves. The combination of these trends reveals an interplay between thermal and catalytic factors. Higher temperatures tend to favor the homogeneous reaction pathway more owing to its stronger temperature sensitivity compared to the heterogeneous reaction, while increasing catalyst activity promotes the heterogeneous mechanism through enhanced surface reaction kinetics. These observations underscore the need to carefully balance thermal and catalytic factors when optimizing HH combustion systems.

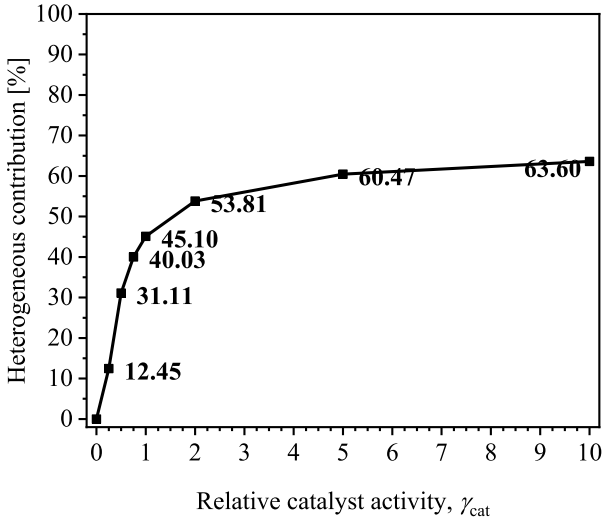

Figure 5. Effect of relative catalyst activity on the HTR contribution.

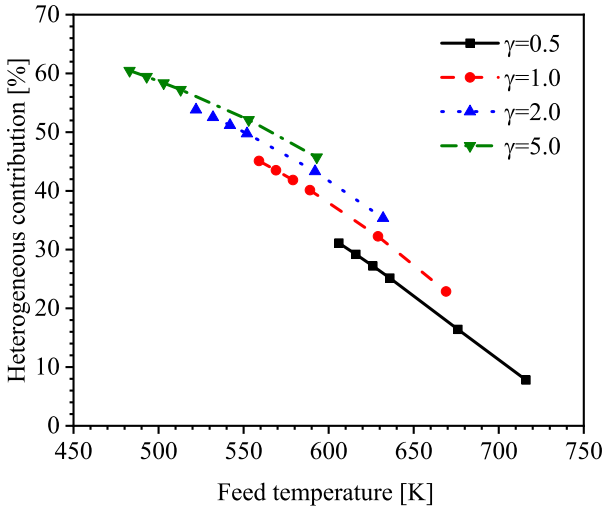

Figure 6. Heterogeneous contribution dependence on catalyst activity and feed temperature.

3.4. Effect of Catalyst Activity on the Ignition Delay Time

Figure 7 illustrates the relationship between the relative catalyst activity and the ignition delay time for the propane/air mixture in the catalytic microreactor. The microreactor is started under cold conditions with an initial temperature of 300 K. The feed temperature is maintained at 10 K above the corresponding ignition temperature for each relative catalyst activity. The independent variable, i.e., relative catalyst activity, ranges from 0.25 to 10 , while the dependent variable, i.e., ignition delay time, decreases from 55.5 s at $\gamma_{cat} = 0.25$ to 21.7 s at $\gamma_{cat} = 10$. The simulation results reveal two distinct regimes: a highly sensitive range between $\gamma_{cat} = 0.25$ and 2, where the ignition time drops from 55.5 s to 28.4 s, and a weakly responsive region from $\gamma_{cat} = 2$ to 10, where the ignition time decreases from 28.4 s to 21.7 s.

This behavior can be attributed to the coupling between reaction kinetics and mass transport limitations. In the low-activity regime, the limited number of active sites on the catalyst results in slower reaction rates, making ignition behavior highly sensitive to increases in catalyst activity. Here, even minor improvements in γ_{cat} significantly reduce the ignition delay time. Conversely, in the high-activity regime, the HTR becomes diffusion-limited rather than kinetically controlled. Due to insufficient reactant flux to active sites, further increases in activity provide diminishing returns by shifting the rate-limiting step

to reactant mass transport toward the catalytic surface. This explains the plateau-like behavior observed at higher γ_{cat} values. The transition between these regimes highlights the interplay between kinetic and transport phenomena in HH combustion systems.

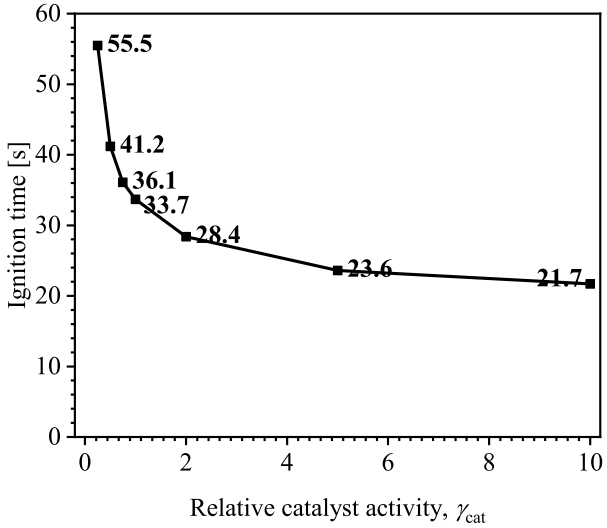

Figure 7. Effect of relative catalyst activity on ignition delay time.

3.5. Effect of Catalyst Activity on the Temporal Evolution of HTR Contribution

Figure 8 depicts the temporal evolution of the HTR contribution in the catalytic microreactor. It can be observed that the HTR accounts for more than 99% of the chemistry during the preheating period because HR is kinetically inhibited at low temperatures. However, continuous heat release from HTR warms the gas mixture. The homogeneous chemistry mechanism engages when the gas mixture temperature crosses the HR activation threshold, driving the heterogeneous share downward until the two reaction routes settle into a stable, coexisting balance. Regardless of the catalytic activity levels, this transition process completes within a remarkably short timeframe. Notably, reduced catalyst activity leads to delayed transition behavior, thereby prolonging the time required to reach steady-state conditions. Meanwhile, the HTR contribution settles at an even lower level. Furthermore, the eventual stabilization of HTR contribution implies a self-regulating mechanism establishing dynamic balance between surface and gas-phase chemistry.

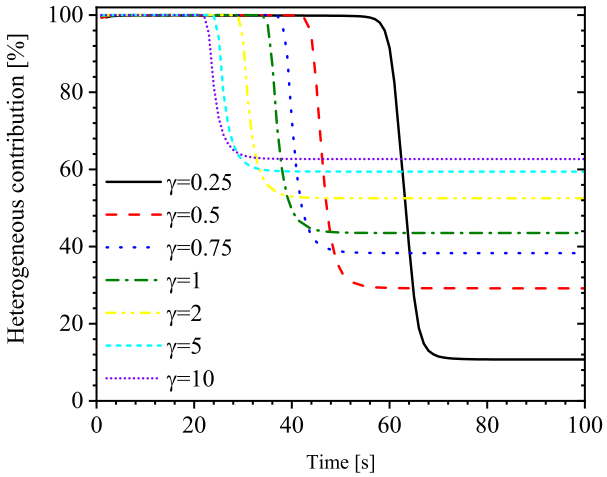

Figure 8. Temporal evolution of heterogeneous reaction contribution.

4. Conclusions

The ignition behavior of catalytic microreactors is a critical research focus for improving small-scale SOFC system startup. This study employs a two-dimensional CFD approach to investigate the ignition characteristics of a propane/air mixture in a Pt-catalyzed microreactor. Numerical computations are performed by varying the surface area factor in the kinetic equation for the catalytic surface reaction, thus examining the effect of catalyst activity. Based on the simulation results, the following key conclusions can be drawn.

(1) As the relative catalyst activity increases from 0 to 10, the ignition temperature of the propane-air mixture decreases significantly from 1063 K to 458 K. The range of 0–2 exhibits high sensitivity, with a dramatic drop of 541 K in ignition temperature. Nevertheless, further increases in activity (2–10) yield a much smaller reduction (64 K), indicating a weakly responsive regime.

(2) Both the maximum combustion temperature and ignition delay time vary with catalyst activity in a manner similar to the trend observed for ignition temperature. Enhancement of catalyst activity is found to inhibit the maximum combustion temperature. The ignition time exhibits high sensitivity to catalyst activity in the relative catalyst activity range of 0–2. For practical applications, targeting this activity range yields optimal ignition time reduction (50% decrease) with minimal catalyst loading.

(3) The initiation of homogeneous ignition undermines the dominance of HTR contribution. Regardless of catalytic activity levels, the relative contributions of the two reaction pathways subsequently undergo dynamic redistribution and ultimately stabilize to reach an equilibrium state within approximately 10 s.

Specifically, we propose that a moderate catalyst activity (e.g., γ_{cat}~0.75–2) likely offers a favorable compromise for preheating, ensuring rapid ignition while avoiding unnecessarily high catalyst loading. This practical range represents the trade-offs among ignition performance, catalyst durability (sintering resistance), and the cost associated with achieving very high Pt dispersion or loading. Possible future work includes incorporating more detailed chemical kinetics for propane/air combustion, accounting for porous washcoat properties, and implementing a sophisticated mass transfer model.

Author Contributions: Conceptualization, Z.W. (Zhulong Wang), Z.L., Z.Y. and G.J.; formal analysis, Z.W. (Zhen Wang), Z.M. and Z.L.; funding acquisition, Z.L. and G.J.; investigation, Z.M., L.M., W.X. and Z.L.; methodology, Z.W. (Zhulong Wang) and Z.W. (Zhen Wang); supervision, Z.Y. and G.J.; writing—original draft, Z.W. (Zhulong Wang) and Z.W. (Zhen Wang); writing—review and editing, Z.Y. and G.J. All authors have read and agreed to the published version of the manuscript.

Funding: This research was supported by the National Natural Science Foundation of China (Grant No. 51876107) and the Research Fund of Binzhou Polytechnic (Grant No. 25-ZJZX-025).

Data Availability Statement: The datasets are made available upon reasonable request to the corresponding author.

Acknowledgments: The authors are grateful to many colleagues with whom they had the privilege to interact and collaborate over the years and whose work is partially referenced in this article.

Conflicts of Interest: The authors declare that the research was conducted in the absence of any commercial or financial relationships that could be construed as a potential conflicts of interest.

References

1. Peng, J.; Huang, J.; Wu, X.; Xu, Y.; Chen, H.; Li, X. Solid oxide fuel cell (SOFC) performance evaluation, fault diagnosis and health control: A review. *J. Power Sources* **2021**, *505*, 230058. [CrossRef]
2. Zheng, K.; Gao, H.; Zhu, M.; Yan, K.; Li, L.; Lin, X.; Wang, Y.; Ni, M. A methane-fueled two-stage SOFC power generation system with carbon capture. *Appl. Therm. Eng.* **2025**, *277*, 127066. [CrossRef]

3. Lin, Z.; Chen, Z.; Jian, J.; Liu, J.; Luo, X.; Liu, Z.; Zhou, J.; Wang, C.; Lei, L.; Liang, B. Ultra-fast and robust startup of a 0.5 W tubular solid oxide fuel cell without thermal insulation. *Int. J. Hydrogen Energy* **2025**, *142*, 180–185. [CrossRef]
4. Eichhorn Colombo, K.W.; Kharton, V.V. Start-up of a solid oxide fuel cell system with a view to materials science-related aspects, control and thermo-mechanical stresses. *Crystals* **2021**, *11*, 732. [CrossRef]
5. Shi, J.; Zhou, D.; Lv, J.; Mao, M.; Ma, X. Self-sustained stable combustion of off-gas from Solid Oxide Fuel Cell in a cone-shaped porous burner with preheaters. *Energy* **2024**, *312*, 133566. [CrossRef]
6. Khanafer, K.; Al-Masri, A.; Vafai, K.; Preethichandra, P. Heat up impact on thermal stresses in SOFC for mobile APU applications: Thermo-structural analysis. *Sustain. Energy Technol. Assess.* **2022**, *52*, 102159. [CrossRef]
7. Li, L.; Wang, S.; Zhao, L.; Fan, A. A numerical investigation on non-premixed catalytic combustion of $CH_4/(O_2+ N_2)$ in a planar micro-combustor. *Fuel* **2019**, *255*, 115823. [CrossRef]
8. Li, L.; Yang, G.; Fan, A. Non-premixed combustion characteristics and thermal performance of a catalytic combustor for micro-thermophotovoltaic systems. *Energy* **2021**, *214*, 118893. [CrossRef]
9. Feng, H.; Zhang, Y.; Liu, J.; Liu, D. Towards heterogeneous catalysis: A review on recent advances of depositing nanocatalysts in continuous-flow microreactors. *Molecules* **2022**, *27*, 8052. [CrossRef]
10. da Silva, J.L., Jr.; Santana, H.S.; Hodapp, M.J. Microreactor technology applied to catalytic processing of Hydrogen: A review. *J. Ind. Eng. Chem.* **2025**, *143*, 65–84. [CrossRef]
11. Fuentes, I.; Mmbaga, J.P.; Hayes, R.E.; Gracia, F. Potential of microreactors for heat transfer efficient CO_2 methanation. *Chem. Eng. Sci.* **2023**, *280*, 119047. [CrossRef]
12. Jiang, L.; Zhang, T.; Sun, S.; Dai, Y.; Mohammed, O.A.H.; Zhang, Y.; Qi, H.; Yang, X.; Xie, M. Visualization on the turbulent structure and restructure characteristic in the wake of a packed bed reactor: PIV measurements and POD analysis. *Renew. Energy* **2025**, *246*, 122895. [CrossRef]
13. Dong, G.; Chen, B.; Liu, B.; Hounjet, L.J.; Cao, Y.; Stoyanov, S.R.; Yang, M.; Zhang, B. Advanced oxidation processes in microreactors for water and wastewater treatment: Development, challenges, and opportunities. *Water Res.* **2022**, *211*, 118047. [CrossRef]
14. Mondal, M.N.A.; Karimi, N.; Jackson, S.D.; Paul, M.C. Impact of catalyst quantity on premixed ultralean hydrogen/air combustion in a packed bed reactor. *Energy Fuels* **2025**, *39*, 9121–9133. [CrossRef]
15. Pan, J.; Zhang, R.; Lu, Q.; Zha, Z.; Bani, S. Experimental study on premixed methane-air catalytic combustion in rectangular micro channel. *Appl. Therm. Eng.* **2017**, *117*, 1–7. [CrossRef]
16. Jiang, L.; Li, M.; Sun, S.; Dai, Y.; Mohammed, O.A.H.; Zhang, Y.; Qi, H.; Yang, X.; Xie, M. Evaluation of stability enhancement and CO reduction in wake reactor at fine combustion States: PIV measurements and POD flame structure analysis. *Chem. Eng. J.* **2025**, *505*, 159633. [CrossRef]
17. Regatte, V.R.; Selle, G.; Kaisare, N.S. The role of homogeneous chemistry during Ignition of propane combustion in Pt-catalyzed microburners. *Int. J. Spray Combust. Dyn.* **2012**, *4*, 155–174. [CrossRef]
18. Chen, J.; Song, W.; Gao, X.; Xu, D. Hetero-/homogeneous combustion and flame stability of fuel-lean propane-air mixtures over platinum in catalytic micro-combustors. *Appl. Therm. Eng.* **2016**, *100*, 932–943. [CrossRef]
19. Di Benedetto, A.; Di Sarli, V.; Russo, G. Effect of geometry on the thermal behavior of catalytic micro-combustors. *Catal. Today* **2010**, *155*, 116–122. [CrossRef]
20. Stefanidis, G.D.; Vlachos, D.G. Controlling homogeneous chemistry in homogeneous-heterogeneous reactors: Application to propane combustion. *Ind. Eng. Chem. Res.* **2009**, *48*, 5962–5968. [CrossRef]
21. Wang, Y.; Yang, W.; Zhou, J.; Yang, H.; Yao, Y.; Cen, K. Heterogeneous reaction characteristics and their effects on homogeneous combustion of methane/air mixture in micro channels I. Thermal analysis. *Fuel* **2018**, *234*, 20–29. [CrossRef]
22. Wang, Y.; Yang, W.; Zhou, J.; Yang, H.; Yao, Y.; Cen, K. Heterogeneous reaction characteristics and its effects on homogeneous combustion of methane/air mixture in microchannels II. Chemical analysis. *Fuel* **2019**, *235*, 923–932. [CrossRef]
23. Kuo, C.H.; Ronney, P.D. Numerical modeling of non-adiabatic heat-recirculating combustors. *Proc. Combust. Inst.* **2007**, *31*, 3277–3284. [CrossRef]
24. Bi, Y.; Li, W.; Zhang, S.; Wang, Z.; Guo, H.; Yu, M.; Li, Z.; Wang, Z. Examining the effects of gap size on ignition characteristics of propane catalytic combustion in a microburner. *J. Phys. Conf. Ser.* **2025**, *2993*, 012035. [CrossRef]
25. Fan, A.; Zhang, H.; Wan, J. Numerical investigation on flame blow-off limit of a novel microscale Swiss-roll combustor with a bluff-body. *Energy* **2017**, *123*, 252–259. [CrossRef]
26. Herdem, M.S.; Mundhwa, M.; Farhad, S.; Hamdullahpur, F. Multiphysics modeling and heat distribution study in a catalytic microchannel methanol steam reformer. *Energy Fuels* **2018**, *32*, 7220–7234. [CrossRef]
27. Herdem, M.S.; Mundhwa, M.; Farhad, S.; Hamdullahpur, F. Catalyst layer design and arrangement to improve the performance of a microchannel methanol steam reformer. *Energy Convers. Manag.* **2019**, *180*, 149–161. [CrossRef]
28. Cao, C.; Zhang, N.; Cheng, Y. Numerical analysis on steam methane reforming in a plate microchannel reactor: Effect of washcoat properties. *Int. J. Hydrogen Energy* **2016**, *41*, 18921–18941. [CrossRef]

29. Liu, W.; Wen, J.; Gong, J.; Liu, G.; Zhong, C.; Pan, J. Parametric study of methane catalytic combustion in a micro-channel reactor: Effects of porous washcoat properties. *Fuel* **2021**, *290*, 120099. [CrossRef]
30. Federici, J.A.; Wetzel, E.D.; Geil, B.R.; Vlachos, D. Single channel and heat recirculation catalytic microburners: An experimental and computational fluid dynamics study. *Proc. Combust. Inst.* **2009**, *32*, 3011–3018. [CrossRef]
31. Zhao, X.; Guo, H.; Li, X.; Han, F.; Wang, B.; Zong, Y.; Wang, Z.; Wang, Z. Impacts of feed temperature on propane ignition features in catalytic micro-burners. *J. Phys. Conf. Ser.* **2025**, *2993*, 012044. [CrossRef]
32. Lu, Q.; Zhou, H.; Zhang, Y.; Gou, J.; Fan, B.; Jiang, C.; Yang, W.; Yuan, J.; Pan, J. Experimental and numerical investigations on hetero-/homogeneous combustion characteristics of C_3H_8/Air mixtures in the micro catalytic combustor. *Appl. Therm. Eng.* **2025**, *274*, 126638. [CrossRef]
33. Regatte, V.R.; Kaisare, N.S. Propane combustion in non-adiabatic microreactors: 1. Comparison of channel and posted catalytic inserts. *Chem. Eng. Sci.* **2011**, *66*, 1123–1131. [CrossRef]
34. Zhang, X.; Miao, Z.; Li, X.; Li, S.; Liu, S.; Wang, Z.; Zhao, Z.; Zhai, W. Numerical studies on the role of wall thermal conductivity in propane ignition features within a catalytic micro-combustor. *J. Phys. Conf. Ser.* **2025**, *3064*, 012014. [CrossRef]
35. Norton, D.G.; Wetzel, E.D.; Vlachos, D.G. Thermal management in catalytic microreactors. *Ind. Eng. Chem. Res.* **2006**, *45*, 76–84. [CrossRef]
36. Di Sarli, V.; Di Benedetto, A. Modeling and simulation of soot combustion dynamics in a catalytic diesel particulate filter. *Chem. Eng. Sci.* **2015**, *137*, 69–78. [CrossRef]
37. Feng, H.; Zhu, X.; Chen, R.; Liao, Q.; Ye, D.; Zhang, B.; Liu, J.; Liu, M.; Chen, G.; Wang, K. pH response of zwitterionic polydopamine layer to palladium deposition in the microchannel. *Chem. Eng. J.* **2019**, *356*, 282–291. [CrossRef]
38. Remmel, A.L.; Ratso, S.; Liivand, K.; Danilson, M.; Kaare, K.; Mikli, V.; Kruusenberg, I. CO_2 transformed into highly active catalysts for the oxygen reduction reaction via low-temperature molten salt electrolysis. *Electrochem. Commun.* **2024**, *166*, 107781. [CrossRef]
39. Najafli, E.; Ratso, S.; Ivanov, Y.P.; Gatalo, M.; Pavko, L.; Yörük, C.R.; Walke, P.; Divitini, G.; Hodnik, N.; Kruusenberg, I. Sustainable CO_2-derived nanoscale carbon support to a platinum catalyst for oxygen reduction reaction. *ACS Appl. Nano Mater.* **2023**, *6*, 5772–5780. [CrossRef]
40. Yang, A.C.; Streibel, V.; Choksi, T.S.; Aljama, H.; Werghi, B.; Bare, S.R.; Sánchez-Carrera, R.S.; Schäfer, A.; Li, Y.; Abild-Pedersen, F.; et al. Insights and comparison of structure–property relationships in propane and propene catalytic combustion on Pd-and Pt-based catalysts. *J. Catal.* **2021**, *401*, 89–101. [CrossRef]
41. Lu, Y.; Deng, H.; Pan, T.; Wang, L.; Zhang, C.; He, H. Interaction between noble metals (Pt, Pd, Rh, Ir, Ag) and defect-enriched TiO_2 and its application in toluene and propene catalytic oxidation. *Appl. Surf. Sci.* **2022**, *606*, 154834. [CrossRef]
42. Lu, Q.; Wang, Q.; Zhang, Y.; Liu, C.; Fan, B.; Nauman, M.; Jiang, C.; Pan, J. Numerical study on methane heterogeneous reaction characteristics in micro catalytic combustors with orthogonal thermal anisotropic walls. *Appl. Therm. Eng.* **2024**, *244*, 122656. [CrossRef]
43. Yedala, N.; Raghu, A.K.; Kaisare, N.S. A 3D CFD study of homogeneous-catalytic combustion of hydrogen in a spiral microreactor. *Combust. Flame* **2019**, *206*, 441–450. [CrossRef]
44. Westbrook, C.K.; Dryer, F.L. Simplified reaction mechanisms for the oxidation of hydrocarbon fuels in flames. *Combust. Sci. Technol.* **1981**, *27*, 31–43. [CrossRef]
45. Deshmukh, S.R.; Vlachos, D.G. A reduced mechanism for methane and one-step rate expressions for fuel-lean catalytic combustion of small alkanes on noble metals. *Combust. Flame* **2007**, *149*, 366–383. [CrossRef]
46. ANSYS FLUENT Inc. *Fluent 14.0 User's Guide*; ANSYS FLUENT Inc.: Canonsburg, PA, USA, 2015.